

DreamSAC: Learning Hamiltonian World Models via Symmetry Exploration

Jinzhou Tang
UC San Diego

tangjzh.ai@gmail.com

Fan Feng
UC San Diego

ffeng1017@gmail.com

Minghao Fu
UC San Diego

isminghaofu@gmail.com

Wenjun Lin
Sun Yat-sen University

linwj59@mail2.sysu.edu.cn

Biwei Huang
UC San Diego

bih007@ucsd.edu

Keze Wang

kezewang@gmail.com

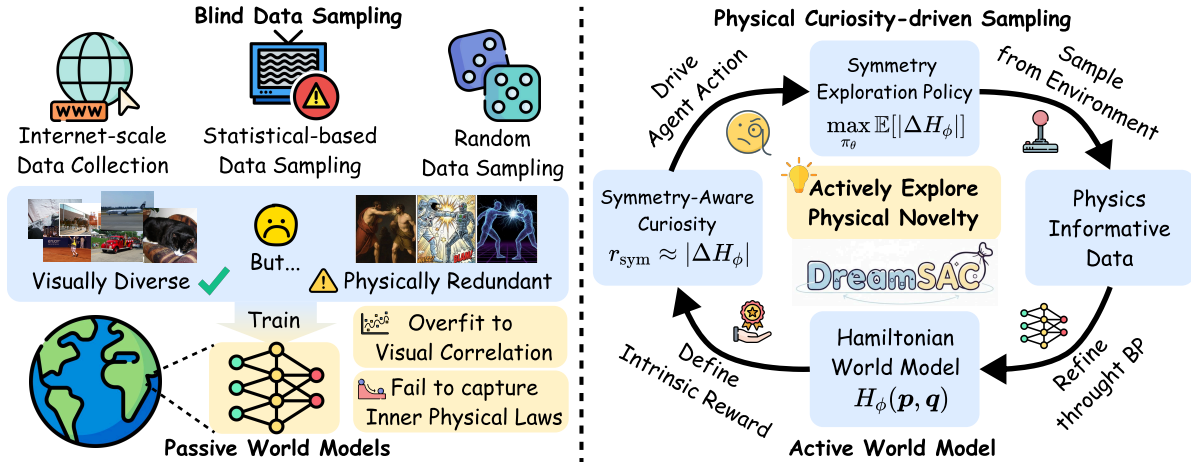


Figure 1. **From passive statistical learning to active physics discovery.** (Left) General world models fail at extrapolation because they are passive learners. They are trained on data that, while potentially visually diverse, is often physically redundant, leading them to learn spurious statistical correlations rather than the environment’s underlying generative rules (e.g., physical laws). (Right) Our framework, DreamSAC, reframes this as an active, interaction-driven process. We introduce Symmetry Exploration, in which the agent is intrinsically motivated by a Hamiltonian-based curiosity to probe and challenge its own understanding of physical laws actively. This process gathers physically informative data for our Hamiltonian World Model, enabling it to discover the environment’s fundamental invariances.

Abstract

Learned world models excel at interpolative generalization but fail at extrapolative generalization to novel physical properties. This limitation arises because they learn statistical correlations rather than the environment’s underlying generative rules, such as physical invariances and conservation laws. We argue that learning these invariances is key to robust extrapolation. To achieve this, we first introduce **Symmetry Exploration**, an unsupervised exploration strategy where an agent is intrinsically motivated by a Hamiltonian-based curiosity bonus to actively probe and challenge its understanding of conservation laws, thereby collecting physically informative data. Second, we design a Hamiltonian-based world model that learns from the collected data, using a novel self-supervised contrastive objective to identify the invariant physical state from raw, view-dependent pixel observations. Our framework, **DreamSAC**,

trained on this actively curated data, significantly outperforms state-of-the-art baselines in 3D physics simulations on tasks requiring extrapolation.

1. Introduction

World models are increasingly central to reinforcement learning (RL), enabling agents to plan from high-dimensional inputs like pixels by building predictive representations of their environment [14, 17, 30, 59]. These models have achieved notable success, demonstrating the ability to generate visually coherent predictions for scenarios involving familiar objects and dynamics, even in novel combinations — the capability often termed *interpolative generalization* [14, 16, 28, 36, 53, 63]. This success comes from their capacity to capture nonparametric statistical patterns within the observed pixel sequences during training.

Despite these successes, a critical limitation persists: the

predictive capabilities of these models often break down drastically when confronted with scenarios involving complex physical interactions [9, 11, 61], particularly those governed by dynamics or parameters different from the training patterns [2, 34], *e.g.*, collisions between objects with unseen mass ratios, novel contact dynamics. Such robustness is essential for agents operating in the unpredictable open world, yet remains a major hurdle [3, 35]. This difficulty reveals a fundamental issue: current models excel at learning the *statistical correlations* of pixel-level dynamics, effectively becoming descriptive systems, but generally failing to capture the underlying *physical laws* or generative rules governing these interactions [8, 10, 21, 40, 43, 46, 57]. Specifically, they operate solely on pixel patterns without an inherent understanding of concepts like force, momentum, or energy conservation [52]. We argue that achieving robust generalization requires shifting the learning objective from modeling pixel statistics towards discovering the environment’s fundamental *physical invariances*, the conservation laws derived from *underlying symmetries*, which inherently govern these interactions [18, 25, 41, 50, 55]. Hence, we posit that explicitly learning these invariances is the key to building world models grounded in physical reality [48, 56].

Building upon this insight, we introduce **DreamSAC** (**Dream** with **Symmetry-Aware Curiosity**, Figure 1), a framework that learns a physics-grounded world model capable of extrapolative generalization. It integrates two core components: First, a *Hamiltonian World Model* H_ϕ that enforces physical symmetries. To reconcile this model’s need for viewpoint-invariant states with viewpoint-dependent pixel inputs, DreamSAC employs a self-supervised contrastive learning objective [26, 60]. This objective places explicit, opposing pressure on the encoder against the reconstruction loss, forcing it to factor out viewpoint variations and isolate a latent state Z_t that represents the underlying invariant physical dynamics [48, 62]. Second, *Symmetry Exploration*, an unsupervised exploration policy designed to iteratively refine this world model. This policy is driven by a novel intrinsic reward, $r_{sym} \approx |\Delta H_\phi|$, calculated directly from the model’s own current and imperfect Hamiltonian H_ϕ . This physics-based curiosity signal motivates the agent to seek interactions that perform the most work (*i.e.*, events predicted to cause the largest energy change). Such interactions are the most effective at exposing the model’s errors in understanding the underlying physics. By efficiently collecting this physically informative data, the agent iteratively corrects H_ϕ , driving its convergence towards the environment’s invariant physical laws.

We validate DreamSAC in 3D physics simulations, demonstrating 22%-163% higher performance over state-of-the-art baselines. Specifically, our framework achieves rapid adaptation to unseen physical parameters (*e.g.*, friction, gravity). Our contributions are mainly three-fold: (1)

Symmetry exploration, an intrinsic motivation for targeted physical data collection; (2) A Hamiltonian world model, trained with a contrastive objective enabling viewpoint-invariant learning from pixels; (3) Comprehensive empirical validation, showcasing DreamSAC’s significant extrapolation capabilities.

2. Related Work

2.1. Structured World Models for RL

Integrating structural inductive biases into world models for Model-Based Reinforcement Learning (MBRL) is an active research area aimed at improving sample efficiency, interpretability, and generalization beyond standard approaches like Dreamer [16]. Common strategies include incorporating physics-based priors derived from classical mechanics (*e.g.*, Hamiltonian or Lagrangian formulations [6, 12, 62]) or learning object-centric representations [51, 58]. However, existing methods face limitations: methods like Dreamer struggle with extrapolation due to their lack of physical grounding [29], while physics-structured models (*e.g.*, HNNs, LNNs) have primarily demonstrated success on low-dimensional state inputs or in offline settings, and their integration into end-to-end agents learning from pixels remains challenging [1, 7, 44]. We address these by embedding a Hamiltonian world model within an online MBRL agent that learns robust dynamics directly from pixel observations through symmetry-aware exploration and contrastive representation learning.

2.2. Self-Supervised Invariant Representations

Learning informative representations from high-dimensional data, such as pixels, is a central challenge in machine learning [13]. A critical requirement for physical systems is learning representations that are *invariant* to nuisance factors, such as camera viewpoint [47] or lighting [54], while retaining all physically salient information. This goal is often in direct conflict with reconstruction-based objectives, which may incentivize the model to encode these very nuisance factors to accurately render the observations [42]. To explicitly enforce invariance, self-supervised contrastive learning has emerged as a dominant and highly effective paradigm [22, 23, 49]. Methods like SimCLR [5] train an encoder to produce similar embeddings for different “augmented” views of the same image (*e.g.*, random crops, color jitter). This mechanism effectively teaches the model to ignore these predefined variations, thereby learning a representation that is robust to them. This principle of using augmentations to build specific invariance provides a powerful tool for disentangling latent factors of variation.

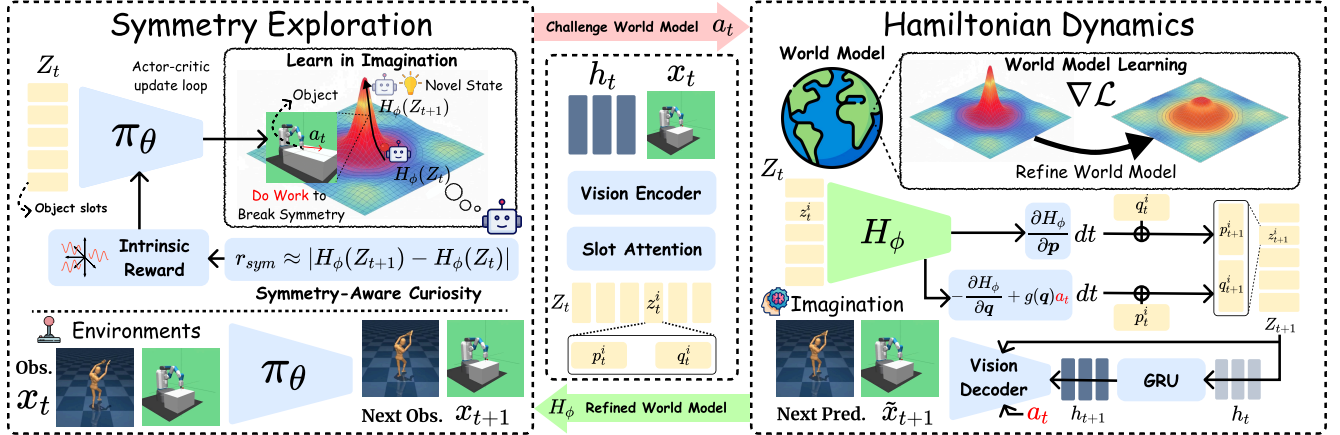


Figure 2. **Overview of DreamSAC.** (Right) Our world model maps observations x_t to object-centric slots Z_t via SAVi [24]. We structure each slot z_t^i into generalized coordinates (q_t^i) and canonical momenta (p_t^i). The dynamics are twofold: the stochastic state Z_{t+1} is computed by integrating our G -invariant Hamiltonian H_ϕ , while the deterministic state h_{t+1} is updated by a GRU. (Left) Symmetry Exploration: To efficiently learn H_ϕ , a policy π_θ is trained entirely in imagination to maximize our Symmetry-Aware Curiosity reward r_{sym} . This incentivizes the policy to work to break symmetry. The imagined policy is then executed in the real environment to collect challenging data, which refines the world model.

2.3. Unsupervised Reinforcement Learning

To learn an accurate world model, an unsupervised agent must be intrinsically motivated to explore its environment [19, 27, 33]. A dominant paradigm is novelty-based curiosity, such as Random Network Distillation (RND) [4] or prediction-error methods (ICM) [39]. These methods reward the agent for visiting statistically novel or unpredictable states. However, a well-known limitation is the “noisy-TV” problem [32], where agents are irreversibly distracted by stochastic elements in the environment [37]. We argue that for learning a physically grounded model, statistical novelty is not effective enough. Instead, our **Symmetry-Aware Curiosity** formalizes a physics-based objective. It does not reward statistical novelty, but rather rewards the agent for performing informative *interactions* [31] that challenge its current understanding of the system’s conservation laws, thus driving it to discover the true Hamiltonian dynamics.

3. Methodology

Our **DreamSAC** is an unsupervised reinforcement learning framework designed to learn world models that are grounded in physical principles, as illustrated in Figure 2. It aims to achieve robust extrapolative generalization by discovering the underlying physical invariances of the environment. The overall architecture is based on the DreamerV3 [17], but we introduce a physics-informed world model and a curiosity-driven learning objective. The entire learning process is divided into two phases: an *unsupervised pretraining phase* driven by our Symmetry Exploration mechanism, followed by a *downstream task adaptation phase* using extrinsic rewards. Full implementation de-

tails, network architectures, and hyperparameters are available in the Supp. 7.

3.1. Preliminaries

Controlled Hamiltonian Dynamics. We model the agent-environment interaction as a controlled Hamiltonian system [62], which separates the system’s **internal dynamics**, governed by an internal Hamiltonian $H_\phi(z)$, from the influence of **external actions** a_t . Given a latent state $z = (q, p)$ representing generalized coordinates and momenta, the internal Hamiltonian $H_\phi(z)$ encodes the system’s energy and underlying physical symmetries. The agent’s action a_t applies an external force via a learned input matrix $g(q)$. The complete dynamics are thus:

$$\frac{dq}{dt} = \frac{\partial H_\phi(z)}{\partial p}, \quad \frac{dp}{dt} = -\frac{\partial H_\phi(z)}{\partial q} + g(q)a_t \quad (1)$$

We solve these equations using a symplectic integrator [48] during inference. Learning an accurate $H_\phi(z)$ is the key to capturing the physical invariances required for extrapolation. Discretizing these continuous-time equations, however, presents a critical trade-off between the gradient stability required for deep generative model training and the long-term physical conservation desired during inference. We address this by employing different integration strategies in training and inference phases (details are in Supp. 6.2).

Invariant Internal Hamiltonian. To encode viewpoint-independent physical laws, we constrain the **internal Hamiltonian** $H_\phi(Z_t)$ to be **invariant** under transformations g from the relevant 3D physical symmetry group G

(e.g., $SE(3)$):

$$H_\phi(g \cdot Z_t) = H_\phi(Z_t), \quad \forall g \in G \quad (2)$$

Here, $Z_t = \{z_t^i\}_{i=1}^N$ is the latent object-centric 3D state. We implement H_ϕ using a G -invariant architecture (i.e., Lie Transformer [20]) that satisfies this property by construction.

The physical meaningfulness of Eq. (2) depends on the encoder q_ϕ learning a **viewpoint-invariant** representation Z_t from the 2D observation x_t , such that $q_\phi(\text{Render}(S, v_1)) \approx q_\phi(\text{Render}(S, v_2)) \approx Z_t$ for a given 3D state S . We explicitly do not require the encoder q_ϕ to be equivariant to *arbitrary* 2D image transformations (e.g., in-plane rotation), which often lack 3D physical meaning. Instead, as detailed in Supp. 6.3, we enforce robustness using a curated set of 2D augmentations (e.g., perspective shifts) that serve as a practical *proxy* for 3D viewpoint changes, and we provide further analysis in Supp. 7.2.

3.2. Hamiltonian World Model

Our contribution is to modify the standard Recurrent State-Space Model (RSSM) [15] to create a Hamiltonian World Model. We argue that the unconstrained, entangled nature of the standard RSSM’s dynamics predictor is a primary cause of failure in extrapolation tasks. Our design aims to disentangle the viewpoint-dependent nature of observations from the viewpoint-independent nature of physical laws.

State Representation and Encoder. We employ an object-centric encoder q_ϕ , based on SAVi [24] (see Supp. 7.2 for architectural details), to map an observation x_t and recurrent state h_t to N object slots $Z_t = \{z_t^i\}_{i=1}^N$. Crucially, we impart physical meaning by structuring each slot to represent its generalized coordinates and momenta, $z_t^i = (q_t^i, p_t^i)$.

While the ELBO (Eq. (5)) provides no formal guarantee that this split corresponds to true canonical coordinates, we hypothesize it creates a **functionally useful decoupling**. This functional decoupling is instead encouraged by the competing objectives within the ELBO: the prediction loss \mathcal{L}_{pred} grounds the entire latent state Z_t in the visual observation x_t , while the Hamiltonian dynamics prior p_ϕ (enforced via \mathcal{L}_{dyn} and \mathcal{L}_{rep}) imposes a strong structural constraint on the *relationship* between the q_t and p_t components as they evolve over time. This reliance on implicit structure learning via generative objectives has shown success in related work [48], and we provide further analysis of the learned representations in Supp. 9.1.

Viewpoint Robustness Constraints. A core challenge in our framework is the conflict between the viewpoint-dependent reconstruction objective \mathcal{L}_{pred} (which drives Z_t

to encode camera parameters to reconstruct x_t) and our G -invariant Hamiltonian prior p_ϕ (which requires Z_t to be invariant to these parameters). Relying solely on the implicit pressure of the ELBO’s KL terms (Eq. (5)) is insufficient.

To resolve this, we introduce a Viewpoint-Robustness Loss (\mathcal{L}_{vr}) based on self-supervised contrastive learning. This approach *does not* require access to privileged, synchronized multi-view data. Instead, it leverages strong *viewpoint augmentations* τ (e.g., random perspective shifts, camera jitter) applied to single observations x_t from the replay buffer.

For each observation x_t in a batch K , we generate two augmented views, $x_t^A = \tau_A(x_t)$ and $x_t^B = \tau_B(x_t)$. These augmentations share the underlying physical content but differ in their nuisance viewpoint parameters. The encoder q_ϕ maps these to latent states $Z_t^A = q_\phi(x_t^A, h_t)$ and $Z_t^B = q_\phi(x_t^B, h_t)$, which form a *positive pair*. All other $K - 1$ representations from the second augmentation set (i.e., Z_j^B where $j \neq t$) serve as *negative pairs*.

$$\mathcal{L}_{vr}(\phi) = -\mathbb{E} \left[\log \frac{\exp(\text{sim}(Z_t^A, Z_t^B)/\tau)}{\sum_{j=1}^K \exp(\text{sim}(Z_t^A, Z_j^B)/\tau)} \right] \quad (3)$$

where $\text{sim}(Z_i, Z_j)$ is a similarity metric (i.e., cosine similarity) and τ is a temperature hyperparameter. This loss explicitly trains the encoder q_ϕ to factor out viewpoint variations, thereby providing a “cleaned”, viewpoint-robust state Z_t that satisfies the requirements of our G -invariant Hamiltonian $H_\phi(Z_t)$.

Hamiltonian Dynamics Prior. Our dynamics prior $p_\phi(Z_{t+1}|Z_t, a_t)$ replaces the standard black-box predictor with a physics-based process grounded in Eq. (1). This process is defined by two learned components: a G -invariant internal Hamiltonian $H_\phi(Z_t)$ (Eq. (2)) and an input matrix network $g(Q_t)$ [62]. We parameterize H_ϕ using a G -invariant architecture (i.e., Lie Transformer [20]) to enforce symmetry by construction. Further architectural details are provided in Supp. 6.2.

These components define the vector field for a **Symplectic Integrator** \mathcal{I} , which deterministically computes the mean of the next state $M_{t+1} = \{\mu_{t+1}^i\}_{i=1}^N = \mathcal{I}(H_\phi, g, Z_t, a_t)$. To ensure compatibility with the variational framework, we model the prior as a factorized Gaussian distribution:

$$p_\phi(Z_{t+1}|Z_t, a_t) = \prod_{i=1}^N \mathcal{N}(z_{t+1}^i; \mu_{t+1}^i, \Sigma_\phi) \quad (4)$$

The mean μ_{t+1}^i is the deterministic, coupled output from the integrator. Crucially, instead of a fixed unit variance (\mathbf{I}), we learn a shared, state-independent diagonal covariance $\Sigma_\phi = \text{diag}(\sigma_\phi^2)$. This provides a more flexible target

for the encoder posterior q_ϕ (within the \mathcal{L}_{rep} KL-divergence) while maintaining tractability. Finally, a standard recurrent model (GRU) updates the deterministic state $h_{t+1} = f_\phi(h_t, Z_t, a_t)$ for use by the decoder and policy networks.

World Model Objective. The world model (ϕ) is trained by maximizing a modified Evidence Lower Bound (ELBO) objective that incorporates our self-supervised robustness loss:

$$\mathcal{L}_{\text{total}}(\phi) = \sum_{t=1}^T \left(\mathcal{L}_{\text{pred}}(\phi) + \beta_{\text{dyn}} \mathcal{L}_{\text{dyn}}(\phi) + \beta_{\text{rep}} \mathcal{L}_{\text{rep}}(\phi) + \gamma \mathcal{L}_{\text{vr}}(\phi) \right) \quad (5)$$

Here, $\mathcal{L}_{\text{pred}} = \mathbb{E}_q[\log p(x_t|Z_t, h_t)]$ is the **reconstruction loss**, which trains the decoder and grounds the latent state Z_t in the observation. The \mathcal{L}_{dyn} and \mathcal{L}_{rep} terms are the dynamics and representation components of the KL divergence, $\text{KL}(q_\phi||p_\phi)$. Following [17], these are split to separately train the Hamiltonian prior (p_ϕ) to predict the encoder’s posterior (q_ϕ), and train the encoder (q_ϕ) to be predictable by the prior. The overall objective thus balances the Prediction Loss (grounding Z_t in x_t) and the Dynamics/Representation Losses (enforcing the Hamiltonian prior). Crucially, the Viewpoint-Robustness Loss (\mathcal{L}_{vr}), weighted by γ , provides the explicit self-supervisory signal to remove viewpoint dependency from Z_t , addressing the core conflict between reconstruction and physical invariance. We refer readers to Supp. 7.1 for the detailed design of these loss functions.

3.3. Unsupervised Symmetry Exploration

Unlike methods learning dynamics from passively observed trajectories, such as SymODEN [62], our unsupervised RL setting requires the agent to **actively explore** its environment to gather informative data for learning the world model (specifically, the internal Hamiltonian H_ϕ). Consequently, a crucial component is an intrinsic motivation mechanism guiding this exploration.

Our exploration strategy stems from a physical insight: to understand a system’s underlying symmetries (encoded by H_ϕ), an agent cannot merely observe its autonomous evolution (where H_ϕ is conserved, $\Delta H \approx 0$). It must **actively probe** the system’s response to external forces (applied via $g(q)a_t$).

Symmetry-Aware Curiosity To learn the Hamiltonian H_ϕ , the agent must actively probe the environment’s physical properties. We propose an intrinsic reward based on the **work** W_C done on the system by the agent’s action, which, per Eq. (1), equals the change in the internal Hamiltonian $|H_\phi(Z_{t+1}) - H_\phi(Z_t)|$.

To encourage temporally coherent exploration rather than high-frequency “jitter”, we also introduce a standard action smoothness regularizer. The physics-based component of our intrinsic reward, r_{sym} , is thus defined as:

$$r_{\text{sym},t+1} = \underbrace{|H_\phi(Z_{t+1}) - H_\phi(Z_t)|}_{\text{Symmetry Probing}} - \underbrace{\lambda_s ||a_t - a_{t-1}||^2}_{\text{Action Smoothness}} \quad (6)$$

where λ_s is a balancing hyperparameter.

This reward function addresses the paradox of learning symmetries: while symmetry implies conservation ($\Delta H \approx 0$), an agent cannot learn this invariance by being passive. It must *actively challenge* the system’s inertia. Maximizing r_{sym} incentivizes the agent to find interactions that require significant work, thereby generating the most informative data for identifying the structural properties (*e.g.*, stiffness, potential barriers) of H_ϕ .

Behavior Learning in Imagination The intrinsic actor-critic ($\pi_\theta, v_{\psi,\text{int}}$) then trains on imagined trajectories following Dreamer [17]. However, the r_{sym} -based objective (Eq. (6)) introduces an instability: r_{sym} is noisy and non-stationary when H_ϕ is untrained, leading to poor data collection. We resolve this by annealing the intrinsic reward from a stable novelty bonus to our physics-based reward.

For this stable bonus, we employ Random Network Distillation (RND) [4], which generates a reward from the agent’s prediction error on its observations against a fixed, randomly initialized target network. This provides a broad and stable novelty signal during the initial phase of training. The final annealed reward is:

$$r_{\text{int},t+1} = (1 - w_t) \cdot r_{\text{RND},t+1} + w_t \cdot r_{\text{sym},t+1} \quad (7)$$

We initialize $w_0 = 0$ (relying fully on RND) to stabilize the world model p_ϕ with diverse data, then linearly anneal $w_t \rightarrow 1$ over T_{anneal} steps. This shifts exploration from novelty-seeking to symmetry-probing as H_ϕ matures. To further mitigate noise, r_{sym} is computed using an EMA target Hamiltonian, H_{target} . This hybrid, annealed reward bootstraps exploration, stabilizing the joint optimization. We refer readers to Supp. 6.4 for more details of these implementations and hyperparameters.

3.4. Downstream Task Adaptation

After unsupervised pretraining, the agent’s world model p_ϕ has learned a dynamics prior that factorizes structural symmetries from implicit physical parameters. To solve any downstream task, we employ a unified adaptation via a fine-tuning strategy as our primary method.

Adaptation via Differentiated Fine-tuning. Our main adaptation strategy is designed to leverage the factored nature of our model. When adapting to a new task (which

Table 1. **World model image prediction accuracy.** We compare the Mean Squared Error (MSE) (lower is better) at 1M steps of our full model against the DreamerV3 [17] baselines (random policy, sample from policy replay buffers) and ablations of our exploration strategy (random policy, RND [4]). Models are evaluated across various DMCS and GymFetch tasks at varying rollout horizons (H).

Method	DeepMind Control Suite										GymFetch				
	Cheetah		Acrobot		Hopper		Walker		Humanoid			FetchPush		FetchReach	
	H=16	H=100	H=16	H=100	H=16	H=100	H=16	H=100	H=5	H=10	H=16	H=8	H=16	H=8	H=16
DreamerV3+Policy	0.7981	0.7507	0.7723	0.9392	1.0355	—	4.3769	—	—	—	—	1.275	2.030	0.855	1.492
DreamerV3+Random	0.8747	0.4048	0.8423	1.7547	0.6406	0.9239	2.2527	4.3760	5.2171	6.0500	6.5078	1.048	1.932	0.962	1.670
DreamerV3+RND	0.6364	0.4578	0.2109	0.5628	1.0643	1.2764	2.8976	3.2160	4.2077	5.7294	6.9389	0.976	1.708	0.574	0.682
DreamSAC+Random	0.1565	0.3367	0.2532	0.9347	0.5227	0.9762	2.4667	3.6391	5.6391	6.1402	6.8589	0.675	0.790	0.498	0.652
DreamSAC (Ours)	0.4052	0.3325	0.2064	0.1806	0.3149	0.5749	1.0044	2.9118	4.7776	5.7798	5.4902	0.302	0.645	0.313	0.386

may have In-Distribution or OOD physical properties), we do not retrain from scratch. Instead, we perform rapid system identification using a differentiated fine-tuning loop: (i) the intrinsic policy π_θ and intrinsic critic $v_{\psi,\text{int}}$ are discarded and re-initialized for the new task; (ii) the viewpoint-robust encoder q_ϕ is kept frozen, as the visual properties of the environment are unchanged; and (iii) the Hamiltonian world model (H_ϕ, g) is fine-tuned with a small learning rate. We hypothesize that H_ϕ 's invariant architecture acts as a strong regularizer, constraining optimization to primarily update implicit physical parameters (e.g., mass, friction) without corrupting the learned symmetries (e.g., $SE(3)$ invariance). This enables far faster adaptation than unstructured models like DreamerV3.

Adaptation Training Loop. The adaptation loop collects new task-specific experiences $(x_t, a_{t-1}, R_{\text{ext},t})$. In each step, the world model p_ϕ updates its fine-tuning parameters (per strategy (iii) above) and its new extrinsic reward predictor $v_{\psi,\text{ext}}$ using the ELBO (Eq. (5)) and a value loss. Simultaneously, the new actor-critic $(\pi_\theta, v_{\psi,\text{ext}})$ updates entirely on imagined trajectories from the fine-tuning world model, maximizing the predicted R_{ext} .

Evaluation of Zero-Shot Generalization. To test the limits of the pretrained model's generalization without any adaptation, we also evaluate its zero-shot capability. For this specific evaluation, we freeze the entire world model p_ϕ (including H_ϕ) and learn a new task-specific policy π_θ entirely within the fixed, pretrained imagination. This tests the model's ability to generalize using only its pretrained understanding of physics.

4. Experiments

Our experimental evaluation is designed to answer three key questions: (1) Does our Hamiltonian world model achieve superior predictive accuracy (Sec. 4.2) compared to baselines? (2) Can this accuracy translate to robust downstream generalization, allowing DreamSAC to outperform baselines on both challenging OOD tasks and standard ID benchmarks (Sec. 4.3)? (3) Are our key contributions,

specifically the Hamiltonian model and symmetry exploration, necessary for this performance (Sec. 4.4), and do they learn the intended physical mechanisms (Sec. 4.5)?

4.1. Experimental Setup

Environments We evaluate our method on a diverse suite of 3D physics benchmarks from DeepMind Control Suite (DMCS) and GymFetch. Our experimental design addresses three distinct goals: (1) To validate *world model performance*, we test prediction MSE on a broad diagnostic suite (e.g., Cheetah, Acrobot, Hopper, Humanoid). (2) To test *extrapolative generalization*, we evaluate OOD performance on a curated set of tasks (Reacher, FetchReach, Walker-walk, Cheetah-run). (3) To measure *downstream task generalization*, we test adaptation on standard control benchmarks (Hopper, Quadruped, Walker). All OOD split definitions and further details are in Supp. 8.

Baselines We compare our full method, DreamSAC, against baselines built from the state-of-the-art world model, DreamerV3 [17], and the state-of-the-art exploration method, RND [4]. Our baseline variants are as follows: (1) DreamerV3+Policy, the standard DreamerV3 model trained on its native policy replay buffer. (2) DreamerV3+Random, the DreamerV3 model trained on data from a random policy. (3) DreamerV3+RND, the DreamerV3 model combined with the RND curiosity bonus. (4) DreamSAC+Random, an ablation of our method using a random exploration policy instead of our Symmetry Exploration.

Implementation Details Our world model is built upon the DreamerV3 JAX codebase. We replace the encoder with a SAVi [24] architecture to obtain object slots Z_t . The dynamics prior p_ϕ is replaced by our Hamiltonian model, where H_ϕ is implemented as a Lie Transformer [20] to enforce $SE(3)$ invariance. All models are pre-trained for 2M environment steps using their respective unsupervised objectives, and then finetuned them 500K steps for downstream tasks for ID and OOD experiments. For our evaluation metrics, we choose the final task reward and the MSE of image reconstruction. We evaluate the MSE at 1M steps,

Table 2. **Comprehensive comparison of extrapolative generalization on all OOD tasks.** We report final performance (Success Rate for FetchReach tasks, Mean Reward for all others) after 2M unsupervised pre-training steps and 500K task adaptation steps (mean \pm std. over 5 seeds). The tasks evaluate **Structural OOD** (Unseen View: new viewpoints, Unseen Object: new object counts, Unseen Goal) and **Parametric OOD** (Unseen Gravity: 1.5x gravity, Unseen Friction: 2.0x friction, Unseen Dist.: physical properties domain shift).

Model	Structural & Interaction Generalization				Parametric Generalization			
	Reacher-hard		FetchReach		Walker-walk		Cheetah-run	
	Unseen View	Unseen Goal	Unseen Object	Unseen Goal	Unseen Gravity	Unseen Dist.	Unseen Friction	Unseen Dist.
DreamerV3+Policy	265.33 \pm 10.33	919.73 \pm 9.12	0.65 \pm 0.12	0.76 \pm 0.11	189.76 \pm 23.27	125.44 \pm 35.70	118.79 \pm 62.23	80.38 \pm 28.43
DreamerV3+RND 0-shot	79.31 \pm 52.98	892.90 \pm 10.37	—	—	86.75 \pm 39.72	34.28 \pm 6.29	9.42 \pm 4.27	7.71 \pm 1.41
DreamerV3+RND	313.97 \pm 27.31	927.36 \pm 18.73	0.70 \pm 0.07	0.72 \pm 0.13	167.52 \pm 21.57	113.40 \pm 32.99	97.43 \pm 67.82	103.42 \pm 27.91
DreamSAC 0-shot	149.64 \pm 37.62	934.21 \pm 7.98	—	—	124.78 \pm 21.77	67.22 \pm 30.13	27.53 \pm 10.98	107.31 \pm 45.41
DreamSAC (Ours)	321.90 \pm 13.28	967.64 \pm 9.29	0.80 \pm 0.09	0.91 \pm 0.04	499.91 \pm 19.77	231.73 \pm 67.08	120.23 \pm 41.26	126.33 \pm 56.59

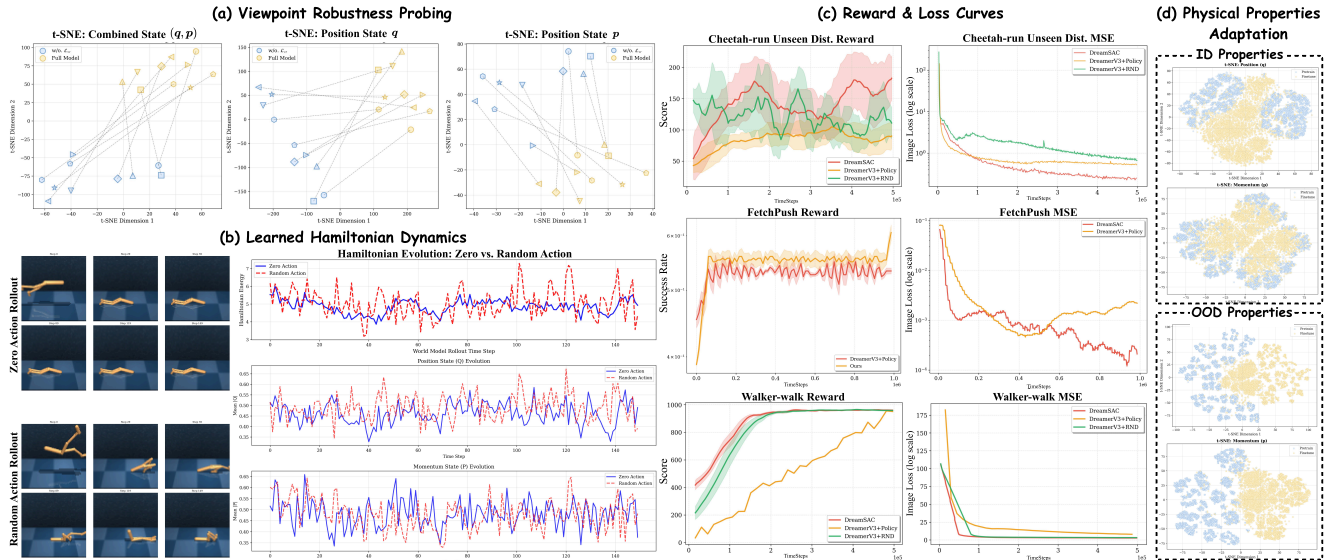


Figure 3. **Qualitative analysis of DreamSAC’s internal mechanisms.** (a) t-SNE projections show our full model (with \mathcal{L}_{VT}) learns viewpoint-invariant representations, unlike an ablation without it. (b) The learned Hamiltonian H_ϕ (red dashed line) is conserved during a zero-action rollout, confirming the model learned a physical invariant (energy conservation). (c) Reward and Loss curves comparing DreamSAC with different baselines. (d) The latent states (q, p) demonstrate physics-awareness: representations for pre-train (yellow) and fine-tune (blue) mix for familiar **In-Distribution** properties, but clearly separate to learn novel **Out-of-Distribution** properties.

as we observed this was a sufficient duration for the predictive loss of all models to have converged. Further details are provided in the Supp. 7.

4.2. World Model Predictive Performance

We first evaluate the foundational predictive accuracy of our Hamiltonian world model against the DreamerV3 baselines. We measure the image prediction Mean Squared Error (MSE) from a rollout conditioned on a single initial image, with results consolidated in Table 1. The results clearly show that DreamSAC (Ours) achieves significantly lower prediction error (lower MSE) than the DreamerV3 baselines across all environments and rollout horizons (H) tested. For instance, in the Acrobot (H=16) environment, our model achieves an MSE of 0.2064, a more than 10x improvement over DreamerV3+Policy’s 3.6390. Similarly, in FetchPush (H=8), our model’s MSE of 0.302 is sub-

stantially lower than DreamerV3+Random’s 1.048, demonstrating a more accurate and stable dynamics model.

Crucially, this table also validates our exploration strategy. Our full model using Symmetry Exploration consistently outperforms other exploration methods. For example, on FetchPush (H=8), our 0.302 MSE is more than twice as accurate as the DreamSAC+Random baseline’s 0.675 and drastically better than the DreamerV3+RND baseline’s 0.976. This demonstrates that our Symmetry-Aware Curiosity actively gathers more physically informative data, which in turn allows the model to learn the underlying dynamics more accurately. This superior predictive accuracy underpins our model’s ability to handle OOD and downstream-task challenges presented in the following sections.

Table 3. **In-Distribution (ID) Task Generalization.** DreamSAC is compared against baselines on standard downstream tasks after pre-training and fine-tuning except for DreamerV3+Policy which is trained from scratch. We report the final Mean Reward (avg. over 5 seeds), showing highly competitive performance.

Method	Hopper		Quadruped		Walker	
	Hop	Stand	Run	Escape	Stand	Walk
DreamerV3+Policy	354.264	929.851	901.963	207.691	903.556	965.217
DreamerV3+RND	389.142	937.651	867.324	179.169	942.684	979.340
DreamSAC (Ours)	366.117	967.865	911.488	236.538	963.251	996.502

4.3. Downstream Task Generalization Performance

Out-of-Distribution (OOD) Generalization We first test OOD performance, our core challenge, with results consolidated in Table 2. DreamSAC consistently outperforms both DreamerV3 and RND baselines across all OOD challenges. On Structural Generalization tasks (columns 1-4), our model’s success rate on FetchReach (Unseen Object, Unseen Goal) clearly surpasses the DreamerV3 baseline. On Reacher-hard, DreamSAC achieves the highest reward on both Unseen View and Unseen Goal, demonstrating a robust advantage over both DreamerV3 and RND. On Parametric Generalization tasks (last four columns), DreamSAC again achieves the highest reward on all Walker-walk and Cheetah-run tasks. The most significant gains are on the Unseen Dist. tasks (physical properties domain shift). This confirms our hypothesis (Sec. 3.4): our differentiated fine-tuning performs rapid system identification on our Hamiltonian parameters. This rapid adaptation is further visualized in Figure 3c, which shows the reward curves for several tasks, where our model (green) mostly learns faster and achieves higher rewards than the baselines (red, orange).

Standard Task Generalization To confirm our model’s applicability as a general-purpose prior, we also evaluate it on standard In-Distribution (ID) downstream control tasks, with results in Table 3. After the same pre-training and fine-tuning process, DreamSAC achieves highly competitive or state-of-the-art performance against both DreamerV3 and RND baselines across all tasks. This demonstrates that our model’s strong physical grounding does not compromise its ability to solve standard control benchmarks.

4.4. Ablation Studies

To validate that our proposed components are necessary, we evaluate three key ablations: (1) Ours (w/o. \mathcal{L}_{vr}), which removes the viewpoint-robustness loss ($\gamma = 0$); (2) Ours (w/o. H_ϕ), which replaces the G -invariant Lie Transformer H_ϕ with a standard MLP; and (3) Ours (w/o. SAVi), which removes the object-centric encoder.

We present a focused evaluation of these ablations on tasks that most directly probe their respective functions in Table 4. The (w/o. \mathcal{L}_{vr}) model’s performance on the

Table 4. **Ablation study of DreamSAC components.** We report final performance on representative OOD tasks. Removing any component causes a significant performance drop on the task it is designed to solve. †Metric is Reward; all other metrics are MSE.

Model	Reacher†	Cheetah	Walker	Avg. OOD
	Unseen View	Seen Env.	1.5x Gravity	MSE
Ours w/o \mathcal{L}_{vr}	212.37 ± 32.47	0.5182	1.0681	0.7932
Ours w/o H_ϕ	159.63 ± 27.12	0.8313	4.9673	2.8993
Ours w/o SAVi	279.68 ± 19.24	0.6179	1.1882	0.9031
DreamSAC (Full)	321.90 ± 13.28	0.4052	1.0044	0.7048

Reacher (Unseen View) task significantly drops, confirming that the contrastive loss is essential for viewpoint invariance. The (w/o. H_ϕ) model, which lacks our Hamiltonian prior, shows a severe performance drop on the Walker (1.5x Gravity) task, demonstrating that the G -invariant architecture is critical for generalizing to new physical parameters. Removing the object-centric encoder (w/o. SAVi) also hurts performance on parametric generalization, confirming all components are essential for robust extrapolation.

4.5. Qualitative Analysis

We provide qualitative visualizations in Figure 3 to confirm our model’s internal mechanisms. First, t-SNE projections (Fig. 3a) show our full model (with \mathcal{L}_{vr}) learns a tight, viewpoint-invariant cluster from different camera views, while an ablation’s representations are scattered, confirming the necessity of our contrastive loss. Second, the learned Hamiltonian H_ϕ (Fig. 3b) remains nearly constant during a zero-action rollout (red dashed line), demonstrating the model has learned a physical invariant (energy conservation). Finally, the t-SNE plots in Figure 3d visualize the physics-aware nature of the learned latent states (q, p). For familiar In-Distribution properties, the fine-tune (blue) and pre-train (yellow) representations remain heavily mixed. In contrast, for novel Out-of-Distribution properties, the fine-tune states form distinct clusters, clearly separating from the pre-train representations. This ability to distinguish between familiar and novel physical properties confirms the model has learned physically meaningful features.

5. Conclusion

In this work, we address the limitation of world models in extrapolative generalization, arguing that they learn statistical correlations rather than underlying physical laws. We introduce DreamSAC, a framework that learns a physically-grounded model through two key innovations: (1) Symmetry Exploration, an unsupervised strategy using Hamiltonian-based curiosity to actively collect physically informative data, and (2) a Hamiltonian World Model with a G -invariant prior. Crucially, we use a self-supervised contrastive loss to force the encoder to learn a viewpoint-

robust latent state, resolving the conflict between reconstruction and physical invariance. Our results confirm that DreamSAC achieves robust generalization to novel poses and views and enables **rapid adaptation to new physical parameters** (via its differentiated fine-tuning), significantly outperforming state-of-the-art baselines.

Acknowledgments

The authors would like to thank Prof. Biwei Huang for the generous support of computing resources. We also thank our colleagues for their helpful discussions and technical support throughout the development of this project.

References

- [1] Mohamadreza Ahmadi, Ufuk Topcu, and Clarence Rowley. Control-oriented learning of lagrangian and hamiltonian systems. In *2018 Annual American Control Conference (ACC)*, pages 520–525, 2018. 2
- [2] Anonymous. Beyond interpolation: Extrapolative reasoning with reinforcement learning and graph neural networks. In *Submitted to The First Workshop on Neural Reasoning and Mathematical Discovery at AAAI’2025*, 2024. under review. 2
- [3] Amirhossein Arzani, Lingxiao Yuan, Pania Newell, and Bei Wang. Interpreting and generalizing deep learning in physics-based problems with functional linear models. *Engineering with Computers*, 41(1):135–157, 2025. 2
- [4] Yuri Burda, Harrison Edwards, Amos Storkey, and Oleg Klimov. Exploration by random network distillation. In *International Conference on Learning Representations*, 2019. 3, 5, 6, 2
- [5] Ting Chen, Simon Kornblith, Mohammad Norouzi, and Geoffrey Hinton. A simple framework for contrastive learning of visual representations. In *Proceedings of the 37th International Conference on Machine Learning*. JMLR.org, 2020. 2
- [6] Miles Cranmer, Sam Greydanus, Stephan Hoyer, Peter Battaglia, David Spergel, and Shirley Ho. Lagrangian neural networks. In *ICLR 2020 Workshop on Integration of Deep Neural Models and Differential Equations*, 2019. 2
- [7] Congyue Deng, Brandon Y. Feng, Cecilia Garraffo, Alan Garbarz, Robin Walters, William T. Freeman, Leonidas Guibas, and Kaiming He. Denoising hamiltonian network for physical reasoning, 2025. 2
- [8] Eva Dierkes, Christian Offen, Sina Ober-Blöbaum, and Kathrin Flaßkamp. Hamiltonian neural networks with automatic symmetry detection. *Chaos: An Interdisciplinary Journal of Nonlinear Science*, 33(6), 2023. 2
- [9] Haoyi Duan, Hong-Xing Yu, Sirui Chen, Li Fei-Fei, and Jiajun Wu. Worldscore: A unified evaluation benchmark for world generation. *arXiv preprint arXiv:2504.00983*, 2025. 2
- [10] Haotian Fu, Yixiang Sun, Michael Littman, and George Konidaris. Knowledge retention in continual model-based reinforcement learning. In *Forty-second International Conference on Machine Learning*. 2
- [11] Alejandro Castañeda Garcia, Jan Warchocki, Jan van Gemert, Daan Brinks, and Nergis Tomen. Learning physics from video: Unsupervised physical parameter estimation for continuous dynamical systems. In *Proceedings of the IEEE/CVF Conference on Computer Vision and Pattern Recognition (CVPR)*, pages 27924–27933, 2025. 2
- [12] Sam Greydanus, Misko Dzamba, and Jason Yosinski. *Hamiltonian neural networks*. Curran Associates Inc., Red Hook, NY, USA, 2019. 2
- [13] Jie Gui, Tuo Chen, Jing Zhang, Qiong Cao, Zhenan Sun, Hao Luo, and Dacheng Tao. A survey on self-supervised learning: Algorithms, applications, and future trends. *IEEE Transactions on Pattern Analysis and Machine Intelligence*, 46(12):9052–9071, 2024. 2
- [14] David Ha and Jürgen Schmidhuber. World models. *arXiv preprint arXiv:1803.10122*, 2(3), 2018. 1
- [15] Danijar Hafner, Timothy Lillicrap, Ian Fischer, Ruben Villegas, David Ha, Honglak Lee, and James Davidson. Learning latent dynamics for planning from pixels. In *International conference on machine learning*, pages 2555–2565. PMLR, 2019. 4
- [16] Danijar Hafner, Jurgis Pasukonis, Jimmy Ba, and Timothy Lillicrap. Mastering diverse domains through world models. *arXiv preprint arXiv:2301.04104*, 2023. 1, 2
- [17] Danijar Hafner, Jurgis Pasukonis, Jimmy Ba, and Timothy Lillicrap. Mastering diverse control tasks through world models. *Nature*, pages 1–7, 2025. 1, 3, 5, 6, 2, 4
- [18] Shuhua Huang, Chenhao Hu, Weiyang Kong, and Yubao Liu. Disentangled contrastive learning for knowledge-aware recommender system. In *The Semantic Web – ISWC 2023: 22nd International Semantic Web Conference, Athens, Greece, November 6–10, 2023, Proceedings, Part I*, page 140–158, Berlin, Heidelberg, 2023. Springer-Verlag. 2
- [19] Adriana Hugessen, Roger Creus Castanyer, and Glen Berseth. Surprise-adaptive intrinsic motivation for unsupervised reinforcement learning. In *Intrinsically-Motivated and Open-Ended Learning Workshop @ NeurIPS2023*, 2023. 3
- [20] Michael J Hutchinson, Charline Le Lan, Shehryar Zaidi, Emilien Dupont, Yee Whye Teh, and Hyunjik Kim. Lietransformer: Equivariant self-attention for lie groups. In *International conference on machine learning*, pages 4533–4543. PMLR, 2021. 4, 6
- [21] Joel Jang, Seonghyeon Ye, Zongyu Lin, Jiannan Xiang, Johan Bjorck, Yu Fang, Fengyuan Hu, Spencer Huang, Kaushil Kundalia, Yen-Chen Lin, et al. Dreamgen: Unlocking generalization in robot learning through video world models. *arXiv preprint arXiv:2505.12705*, 2025. 2
- [22] Bingyi Kang, Yang Yue, Rui Lu, Zhijie Lin, Yang Zhao, Kaixin Wang, Gao Huang, and Jiashi Feng. How far is video generation from world model: A physical law perspective. *arXiv preprint arXiv:2411.02385*, 2024. 2
- [23] Asifullah Khan, Laiba Asmatullah, Anza Malik, Shahzaib Khan, and Hamna Asif. A survey on self-supervised contrastive learning for multimodal text-image analysis, 2025. 2
- [24] Thomas Kipf, Gamaleldin F Elsayed, Aravindh Mahendran, Austin Stone, Sara Sabour, Georg Heigold, Rico Jon-

- schkowsky, Alexey Dosovitskiy, and Klaus Greff. Conditional object-centric learning from video. *arXiv preprint arXiv:2111.12594*, 2021. 3, 4, 6
- [25] Kenneth Li, Aspen K Hopkins, David Bau, Fernanda Viégas, Hanspeter Pfister, and Martin Wattenberg. Emergent world representations: Exploring a sequence model trained on a synthetic task. *ICLR*, 2023. 2
- [26] Zheng Li, Pei Qu, Yufei Jia, Shihui Zhou, Haizhou Ge, Jiahang Cao, Jinni Zhou, Guyue Zhou, and Jun Ma. Manivid-3d: Generalizable view-invariant reinforcement learning for robotic manipulation via disentangled 3d representations. *ArXiv*, abs/2509.11125, 2025. 2
- [27] Aly Lidayan, Michael D Dennis, and Stuart Russell. BAMDP shaping: a unified theoretical framework for intrinsic motivation and reward shaping. In *The Thirteenth International Conference on Learning Representations*, 2025. 3
- [28] Yuren Liu, Biwei Huang, Zhengmao Zhu, Honglong Tian, Mingming Gong, Yang Yu, and Kun Zhang. Learning world models with identifiable factorization. *Advances in Neural Information Processing Systems*, 36:31831–31864, 2023. 1
- [29] Michael Lutter, Johannes Silberbauer, Joe Watson, and Jan Peters. Differentiable physics models for real-world offline model-based reinforcement learning. In *2021 IEEE International Conference on Robotics and Automation (ICRA)*, page 4163–4170. IEEE Press, 2021. 2
- [30] Jiangran Lyu, Ziming Li, Xuesong Shi, Chaoyi Xu, Yizhou Wang, and He Wang. DyWA: Dynamics-adaptive world action model for generalizable non-prehensile manipulation. In *ICRA 2025 Workshop: Beyond Pick and Place*, 2025. 1
- [31] Fryderyk Mantiuk, Hanqi Zhou, and Charley M. Wu. From curiosity to competence: How world models interact with the dynamics of exploration, 2025. 3
- [32] Augustine Mavor-Parker, Kimberly Young, Caswell Barry, and Lewis Griffin. How to stay curious while avoiding noisy TVs using aleatoric uncertainty estimation. In *Proceedings of the 39th International Conference on Machine Learning*, pages 15220–15240. PMLR, 2022. 3
- [33] Russell Mendonca, Oleh Rybkin, Kostas Daniilidis, Danijar Hafner, and Deepak Pathak. Discovering and achieving goals via world models. *Advances in Neural Information Processing Systems*, 34:24379–24391, 2021. 3
- [34] Victor RF Miranda, Armando A Neto, Gustavo M Freitas, and Leonardo A Mozelli. Generalization in deep reinforcement learning for robotic navigation by reward shaping. *IEEE Transactions on Industrial Electronics*, 71(6):6013–6020, 2023. 2
- [35] Kohei Noda, Araki Wakiuchi, Yoshihiro Hayashi, and Ryo Yoshida. Advancing extrapolative predictions of material properties through learning to learn. *arXiv preprint arXiv:2404.08657*, 2024. 2
- [36] Minting Pan, Xiangming Zhu, Yunbo Wang, and Xiaokang Yang. Iso-dream: Isolating and leveraging noncontrollable visual dynamics in world models. In *Neural Information Processing Systems*, 2022. 1
- [37] Yiyuan Pan, Zhe Liu, and Hesheng Wang. Wonder wins ways: Curiosity-driven exploration through multi-agent contextual calibration, 2025. 3
- [38] Deepak Pathak, Pulkit Agrawal, Alexei A Efros, and Trevor Darrell. Curiosity-driven exploration by self-supervised prediction. In *International conference on machine learning*, pages 2778–2787. PMLR, 2017. 6
- [39] Deepak Pathak et al. Curiosity-driven exploration by self-supervised prediction. In *ICML*, 2017. 3
- [40] Pai Peng, Xiaoyang Huang, Chao Yin, Linta Joseph, Chandrasekhar Ramanathan, and Paola Cappellaro. Deep reinforcement learning for quantum hamiltonian engineering. *Physical Review Applied*, 18(2):024033, 2022. 2
- [41] Jordan Peper, Zhenjiang Mao, Yuang Geng, Siyuan Pan, and Ivan Ruchkin. Four principles for physically interpretable world models. In *ICRA 2025 Workshop on Foundation Models and Neuro-Symbolic AI for Robotics*. 2
- [42] Senthil Purushwalkam and Abhinav Gupta. Demystifying contrastive self-supervised learning: invariances, augmentations and dataset biases. In *Proceedings of the 34th International Conference on Neural Information Processing Systems*, Red Hook, NY, USA, 2020. Curran Associates Inc. 2
- [43] Julian Quevedo, Percy Liang, and Sherry Yang. Evaluating robot policies in a world model. *arXiv preprint arXiv:2506.00613*, 2025. 2
- [44] Robin Schiewer, Anand Subramoney*, and Laurenz Wiskott*. Exploring the limits of hierarchical world models in reinforcement learning. *Scientific Reports*, 14(1):26856, 2024. 2
- [45] Ramanan Sekar et al. Planning to explore via self-supervised world models. In *ICML*, 2020. 6
- [46] Torbjørn Smith and Olav Egeland. Learning hamiltonian dynamics with reproducing kernel hilbert spaces and random features. *European Journal of Control*, 80:101128, 2024. 2
- [47] Yonglong Tian, Chen Sun, Ben Poole, Dilip Krishnan, Cordelia Schmid, and Phillip Isola. What makes for good views for contrastive learning? In *Proceedings of the 34th International Conference on Neural Information Processing Systems*, Red Hook, NY, USA, 2020. Curran Associates Inc. 2
- [48] Peter Toth, Danilo J Rezende, Andrew Jaegle, Sébastien Racanière, Aleksandar Botev, and Irina Higgins. Hamiltonian generative networks. In *International Conference on Learning Representations*. 2, 3, 4
- [49] Aäron van den Oord, Yazhe Li, and Oriol Vinyals. Representation learning with contrastive predictive coding. *ArXiv*, abs/1807.03748, 2018. 2
- [50] Miguel Vaquero, Jorge Cortés, and David Martín de Diego. Symmetry preservation in hamiltonian systems: simulation and learning. *Journal of Nonlinear Science*, 34(6):115, 2024. 2
- [51] Rishi Veerapaneni, John D. Co-Reyes, Michael Chang, Michael Janner, Chelsea Finn, Jiajun Wu, Joshua Tenenbaum, and Sergey Levine. Entity abstraction in visual model-based reinforcement learning. In *Proceedings of the Conference on Robot Learning*, pages 1439–1456. PMLR, 2020. 2
- [52] Fei Wang, Liping Chen, and Jianwan Ding. Symplectic physics-embedded learning via lie groups hamiltonian formulation for serial manipulator dynamics prediction. *Scientific Reports*, 15(1):33179, 2025. 2

- [53] Qi Wang, Junming Yang, Yunbo Wang, Xin Jin, Wenjun Zeng, and Xiaokang Yang. Making offline rl online: Collaborative world models for offline visual reinforcement learning. *Advances in Neural Information Processing Systems*, 37:97203–97230, 2024. [1](#)
- [54] Zhixiang Wei, Lin Chen, Tao Tu, Pengyang Ling, Huaian Chen, and Yi Jin. Disentangle then parse: Night-time semantic segmentation with illumination disentanglement. In *Proceedings of the IEEE/CVF International Conference on Computer Vision*, pages 21593–21603, 2023. [2](#)
- [55] Matthias Weissenbacher, Samarth Sinha, Animesh Garg, and Kawahara Yoshinobu. Koopman q-learning: Offline reinforcement learning via symmetries of dynamics. In *Proceedings of the 39th International Conference on Machine Learning*, pages 23645–23667. PMLR, 2022. [2](#)
- [56] Matthias Weissenbacher, Rishabh Agarwal, and Yoshinobu Kawahara. Sit: symmetry-invariant transformers for generalisation in reinforcement learning. In *Proceedings of the 41st International Conference on Machine Learning*, pages 52695–52719, 2024. [2](#)
- [57] Jialong Wu, Shaofeng Yin, Ningya Feng, Xu He, Dong Li, Jianye Hao, and Mingsheng Long. ivideoopt: Interactive videoopt are scalable world models. *Advances in Neural Information Processing Systems*, 37:68082–68119, 2024. [2](#)
- [58] Ziyi Wu, Nikita Dvornik, Klaus Greff, Thomas Kipf, and Animesh Garg. Slotformer: Unsupervised visual dynamics simulation with object-centric models. In *The Eleventh International Conference on Learning Representations*, 2023. [2](#)
- [59] Yingchen Xu, Jack Parker-Holder, Aldo Pacchiano, Philip Ball, Oleh Rybkin, Tim Rocktäschel, and Edward Grefenstette. Learning general world models in a handful of reward-free deployments. *Advances in Neural Information Processing Systems*, 35:26820–26838, 2022. [1](#)
- [60] Zhecheng Yuan, Tianming Wei, Shuiqi Cheng, Gu Zhang, Yuanpei Chen, and Huazhe Xu. Learning to manipulate anywhere: A visual generalizable framework for reinforcement learning. In *8th Annual Conference on Robot Learning*, 2024. [2](#)
- [61] Jiahao Zhang, Muqing Jiang, Nanru Dai, Taiming Lu, Arda Uzunoglu, Shunchi Zhang, Yana Wei, Jiahao Wang, Vishal M Patel, Paul Pu Liang, et al. World-in-world: World models in a closed-loop world. *arXiv preprint arXiv:2510.18135*, 2025. [2](#)
- [62] Yaofeng Desmond Zhong, Biswadip Dey, and Amit Chakraborty. Symplectic ode-net: Learning hamiltonian dynamics with control. In *International Conference on Learning Representations*. [2](#), [3](#), [4](#), [5](#)
- [63] Siyuan Zhou, Yilun Du, Jiaben Chen, Yandong Li, Dit-Yan Yeung, and Chuang Gan. Robodreamer: learning compositional world models for robot imagination. In *Proceedings of the 41st International Conference on Machine Learning*, pages 61885–61896, 2024. [1](#)

DreamSAC: Learning Hamiltonian World Models via Symmetry Exploration

Supplementary Material

6. Detailed Methodology

6.1. Work as Symmetry Breaking

Our symmetry-aware exploration aims to learn the internal Hamiltonian H_ϕ , which encodes the system’s conservative dynamics and symmetries. By Noether’s theorem, continuous symmetries in a physical system correspond to conserved quantities. For an autonomous (closed) Hamiltonian system, time-translation symmetry implies conservation of energy, meaning the Hamiltonian is constant along trajectories:

$$\begin{aligned} \frac{dH}{dt} &= \frac{\partial H}{\partial q} \dot{q} + \frac{\partial H}{\partial p} \dot{p} \\ &= \frac{\partial H}{\partial q} \left(\frac{\partial H}{\partial p} \right) + \frac{\partial H}{\partial p} \left(-\frac{\partial H}{\partial q} \right) = 0 \end{aligned} \quad (8)$$

In such a closed system, observing passive evolution provides limited information about the underlying structure of H , as the system remains on a fixed energy level set.

To efficiently learn H across its entire domain, an agent must actively break this conservation. In our controlled setting (Eq. 11), the agent’s action a_t acts as a non-conservative external force. The time evolution of the Hamiltonian in this open system becomes:

$$\begin{aligned} \frac{dH}{dt} &= \frac{\partial H}{\partial q} \dot{q} + \frac{\partial H}{\partial p} \dot{p} \\ &= \frac{\partial H}{\partial q} \left(\frac{\partial H}{\partial p} \right) + \frac{\partial H}{\partial p} \left(-\frac{\partial H}{\partial q} + g(q)a_t \right) \end{aligned} \quad (9)$$

Simplifying this yields a direct relationship between the change in the Hamiltonian and the external work done by the agent:

$$\frac{dH}{dt} = \left[\frac{\partial H}{\partial p} \right]^\top g(q)a_t = \dot{q}^\top F_{ext} = P_{ext} \quad (10)$$

where $F_{ext} = g(q)a_t$ is the effective external force and P_{ext} is the external power delivered to the system.

Equation (10) provides the theoretical justification for our intrinsic reward, $r_{sym} \approx |\Delta H|$. By maximizing $|H(Z_{t+1}) - H(Z_t)|$, the agent is intrinsically motivated to perform actions that maximize work done on or by the system. This actively steers the system away from its current energy level sets, effectively “breaking” the symmetries that hold for unforced trajectories and exploring new regions of the phase space essential for robustly learning the global structure of H_ϕ .

6.2. Hamiltonian Dynamics and Discretization

Our world model’s latent dynamics follow the controlled Hamiltonian equations of motion. In continuous time, for a latent state $Z = (\mathbf{q}, \mathbf{p})$ and control action a_t , these are:

$$\begin{aligned} \dot{q} &= \frac{\partial H_\phi}{\partial p}(\mathbf{q}, \mathbf{p}) \\ \dot{p} &= -\frac{\partial H_\phi}{\partial q}(\mathbf{q}, \mathbf{p}) + g_\phi(q)a_t \end{aligned} \quad (11)$$

Dual Integration Strategy. Discretizing these equations requires careful consideration. While Symplectic Integrators are essential for long-term energy conservation, they can sometimes yield less stable gradients during the early phases of training deep generative models compared to standard numerical methods. To balance training stability with physical faithfulness during imagination, we employ a dual integration strategy:

- **World Model Training (Gradient Stability):** During the pretraining and adaptation phases, where we optimize the world model parameters ϕ via the ELBO (short-horizon predictions), we employ a standard explicit Euler integrator for maximum gradient stability and computational efficiency.
- **Imagination & Inference (Physical Conservation):** During actor-critic training (imagined rollouts) and evaluation, where long-horizon physical consistency is paramount, we switch to the explicit Symplectic Leapfrog Integrator.

Discussion of Limitations. We acknowledge that optimizing the vector field under Euler discretization while evaluating it with Leapfrog introduces a theoretical gap: the model is not strictly “trained to be symplectic.” However, this is a deliberate design choice. Training directly through a multi-step Symplectic Integrator can lead to exploding gradients in the early stages of learning deep generative models. By using a small time step Δt , the discretization error between Euler and Leapfrog is minimized. Empirically, we find that the vector field learned via Euler approximation sufficiently captures the underlying continuous Hamiltonian dynamics. Crucially, with our sufficiently small integration step ($\Delta t = 0.1$), the learned dynamics approach the continuous ODE limit. This ensures that the Symplectic Integrator utilized during inference theoretically guarantees the preservation of symplectic structure and energy conservation, rendering it a structurally grounded choice rather than merely an empirical heuristic.

Explicit Leapfrog with Control. Despite using a general parameterized Hamiltonian $H_\phi(q, p)$, our network architecture ensures efficient computation of partial derivatives via automatic differentiation, allowing for an explicit approximation. We apply the control input a_t (assumed constant over Δt) during both momentum half-steps. The update from (q_t, p_t) to (q_{t+1}, p_{t+1}) is:

1. **Half-step Momentum Update:**

$$p_{t+1/2} = p_t + \frac{\Delta t}{2} \left(-\frac{\partial H_\phi}{\partial q}(q_t, p_t) + g_\phi(q_t) a_t \right) \quad (12)$$

2. **Full-step Position Update:**

$$q_{t+1} = q_t + \Delta t \cdot \frac{\partial H_\phi}{\partial p}(q_t, p_{t+1/2}) \quad (13)$$

3. **Full-step Momentum Completion:**

$$p_{t+1} = p_{t+1/2} + \frac{\Delta t}{2} \left(-\frac{\partial H_\phi}{\partial q}(q_{t+1}, p_{t+1/2}) + g_\phi(q_{t+1}) a_t \right) \quad (14)$$

This formulation ensures that the external work done by the agent is correctly accounted for in the system’s momentum change while preserving the symplectic structure of the internal dynamics during rollout.

6.3. Viewpoint-Robustness

To ensure the latent state Z_t captures underlying physical dynamics rather than nuisance viewpoint parameters, we employ a self-supervised contrastive loss, \mathcal{L}_{vr} . This loss explicitly incentivizes the encoder q_ϕ to be invariant to image transformations that preserve the physical state.

Augmentation Pipeline. We construct positive pairs (x_t^A, x_t^B) from a single observation x_t by applying a stochastic sequence of augmentations. To effectively simulate complex viewpoint changes and environmental variations, we utilize the following augmentations in order (all implemented using standard TorchVision transforms):

- **Random Resized Crop:** Simulates changes in camera distance and focus. We use a scale range of [0.8, 1.0] and an aspect ratio range of [0.75, 1.33].
- **Random Perspective:** Crucial for simulating drastic camera angle shifts. We use a distortion scale of 0.5 applied with a probability of 0.5.
- **Color Jitter:** Simulates lighting variations. We adjust brightness, contrast, saturation, and hue with factors of [0.4, 0.4, 0.4, 0.1] respectively, applied with probability 0.8.
- **Gaussian Blur:** Prevents reliance on high-frequency artifacts. We use a kernel size of 23 (roughly 10% of image size) and a sigma range of [0.1, 2.0], applied with probability 0.5.

Loss Implementation Details. We adopt the InfoNCE loss. For a minibatch of size K , we use the other $2(K - 1)$ augmented views within the same batch as negative samples. No external memory bank is used. For a positive pair (i, j) , the loss is:

$$\ell_{i,j} = -\log \frac{\exp(\text{sim}(Z_i, Z_j)/\tau)}{\sum_{k=1, k \neq i}^{2K} \exp(\text{sim}(Z_i, Z_k)/\tau)} \quad (15)$$

where $\text{sim}(u, v)$ is cosine similarity.

Temperature Parameter τ Analysis. The temperature parameter τ controls the sharpness of the distribution and the "hardness" of negative samples. We use $\tau = 0.07$ for all main experiments. Table 5 shows a sensitivity analysis on the 'FetchPush New View' task, demonstrating that our chosen value provides an optimal balance between learning discriminative features and training stability.

Preserving Physical Signal under Augmentation. A critical concern is whether strong visual augmentations might degrade the model’s ability to identify fine-grained physical properties (e.g., mass or friction) required for parametric generalization. We address this by strictly limiting our augmentation pipeline to **spatial and chromatic transformations** (e.g., crop, perspective, color) while strictly forbidding temporal augmentations (e.g., frame skipping, speed jitter). Since physical parameters like mass are inferred from the *temporal evolution* of the state (i.e., acceleration under force), our strategy ensures that the temporal structure remains intact. The contrastive loss \mathcal{L}_{vr} thus forces the encoder to discard static visual nuisances (viewpoint) while retaining the temporal dynamics information essential for the Hamiltonian world model to infer implicit physical parameters.

Table 5. Sensitivity analysis of the temperature parameter τ on Reacher Hard (Unseen View) mean reward (mean over 5 seeds).

Temperature τ	0.05	0.07 (Ours)	0.1	0.2	0.5
Mean Reward	312.4	321.9	308.7	245.3	112.8

6.4. Symmetry Exploration Reward Annealing

The intrinsic reward $r_{int,t}$ combines a standard novelty-based exploration bonus (r_{RND}) and our proposed physics-based symmetry probing bonus (r_{sym}). Since these two signals originate from different sources (prediction error vs. Hamiltonian difference) and fluctuate significantly during training, proper normalization is crucial.

Following the standard practice in Dreamer [17] and RND [4], we normalize each reward component using

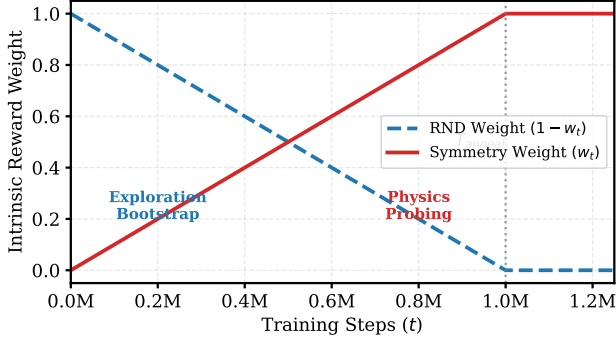


Figure 4. Visual illustration of the linear annealing schedule for an environment with $T_{anneal} = 10^6$.

its **running standard deviation**. We maintain a running standard deviation σ_i for each reward stream $i \in \{RND, sym\}$. The normalized rewards used in the annealing equation are calculated as:

$$\tilde{r}_{i,t} = \frac{r_{i,t}}{\sigma_{i,t}} \quad (16)$$

The final annealed reward is then computed as:

$$r_{int,t} = (1 - w_t) \cdot \tilde{r}_{RND,t} + w_t \cdot \tilde{r}_{sym,t} \quad (17)$$

This dynamic normalization ensures that the magnitude of the intrinsic rewards remains consistent (≈ 1.0) throughout the training process, preventing either component from dominating the learning signal due to scale differences.

Rationale for Annealing. At the beginning of training, the Hamiltonian world model H_ϕ is randomly initialized. Consequently, the symmetry probing reward $r_{sym,t} \propto |H_\phi(Z_{t+1}) - H_\phi(Z_t)|$ is extremely noisy and does not yet reflect true physical information gain. Relying solely on it initially can lead to degenerate exploration behaviors. To bootstrap the learning process, we initially rely on r_{RND} . We use a standard RND implementation that operates directly on pixel observations, providing a stable, model-agnostic diversity signal. This ensures broad coverage of the state space, collecting the initial data necessary to start training H_ϕ . As H_ϕ becomes more accurate, we linearly shift the exploration focus towards active symmetry probing.

Annealing Schedule. We employ a linear annealing schedule for the weight w_t :

$$w_t = \text{clip}\left(\frac{t}{T_{anneal}}, 0, 1\right) \quad (18)$$

The annealing duration T_{anneal} is a task-dependent hyperparameter, generally set longer for environments with more

complex dynamics that require more initial data to stabilize H_ϕ . Table 6 lists the specific values used.

Table 6. Annealing duration T_{anneal} for different environments. We set longer annealing phases for environments with complex dynamics or high-dimensional state spaces (e.g., Humanoid, Quadruped) to allow sufficient exploration via RND before switching to symmetry probing.

Environment	T_{anneal} (Steps)
<i>GymFetch Manipulation</i>	
FetchReach	2×10^5
FetchPush	5×10^5
FetchSlide	1×10^6
<i>DeepMind Control Suite</i>	
Acrobot Swingup	2×10^5
Reacher Hard	5×10^5
Hopper Hop	5×10^5
Walker Walk / Run	5×10^5
Cheetah Run	5×10^5
Quadruped Run / Escape	1×10^6
Humanoid Walk	1×10^6

7. Implementation Details

7.1. World Model Loss Functions

Our full world model objective (Eq. 5 in the main paper) is:

$$\mathcal{L}_{total}(\phi) = \sum_{t=1}^T \left(\mathcal{L}_{pred}(\phi) + \beta_{dyn} \mathcal{L}_{dyn}(\phi) + \beta_{rep} \mathcal{L}_{rep}(\phi) + \gamma \mathcal{L}_{vr}(\phi) \right)$$

As we introduce a novel Hamiltonian dynamics prior, p_ϕ , the standard KL divergence losses from [17] must be adapted. We define these components as follows:

Prediction Loss (\mathcal{L}_{pred}) This is the standard reconstruction loss, formulated as the log-likelihood of the observation x_t given the latent state Z_t and the recurrent state h_t :

$$\mathcal{L}_{pred} = -\mathbb{E}_{q_\phi(Z_t|x_t,h_t)} [\log p_\phi(x_t|Z_t, h_t)]$$

where $q_\phi(Z_t|x_t, h_t)$ is the posterior from the object-centric encoder, and $p_\phi(x_t|Z_t, h_t)$ is the decoder.

Dynamics and Representation Losses ($\mathcal{L}_{dyn}, \mathcal{L}_{rep}$)

These are the two components of the KL divergence that force the latent state Z_t inferred from the image (the posterior q_ϕ) to match the state predicted by the Hamiltonian

dynamics (the prior p_ϕ). Our key modification is that our prior p_ϕ is Markovian on Z and does not depend on the recurrent state h_t .

The posterior q_ϕ is inferred from the current image x_t and history h_t . The prior p_ϕ is predicted from the previous latent state Z_{t-1} and action a_{t-1} using our Hamiltonian integrator (Eq. 4).

Following [17], we split the KL divergence and apply stop-gradients (sg) to create two distinct losses that train the encoder and the prior separately:

$$\mathcal{L}_{dyn} = KL[\text{sg}(q_\phi(Z_t|x_t, h_t)) \parallel p_\phi(Z_t|Z_{t-1}, a_{t-1})]$$

This loss trains the Hamiltonian prior p_ϕ (i.e., H_ϕ) to correctly predict the latent state Z_t that the encoder inferred from the image.

$$\mathcal{L}_{rep} = KL[q_\phi(Z_t|x_t, h_t) \parallel \text{sg}(p_\phi(Z_t|Z_{t-1}, a_{t-1}))]$$

This loss trains the encoder q_ϕ to produce latent states Z_t that are consistent with the predictions of the (fixed) dynamics prior. Following DreamerV3 [17], we do not use fixed static weights for \mathcal{L}_{dyn} and \mathcal{L}_{rep} . Instead, we employ KL Balancing to encourage the posterior to maintain sufficient entropy while pulling the prior towards it. The objective is computed as:

$$\mathcal{L}_{KL} = \beta_{dyn} KL[\text{sg}(q_\phi) \parallel p_\phi] + \beta_{rep} KL[q_\phi \parallel \text{sg}(p_\phi)] \quad (19)$$

We set the coefficients to $\beta_{dyn} = 0.5$ and $\beta_{rep} = 0.1$. This configuration allows the prior to learn the dynamics rapidly without collapsing the posterior’s representation capacity, ensuring the Hamiltonian structure H_ϕ captures rich physical features from the start.

7.2. Network Architectures

7.2.1. Object-Centric Encoder (SAVi)

We utilize the Slot Attention for Video (SAVi) [24] architecture to decompose the visual scene into object-centric latent slots $Z_t = \{z_t^1, \dots, z_t^N\}$.

- **Backbone:** A ResNet-18 (truncated) extracts a feature map of size $H' \times W' \times D_{enc}$ from the 64×64 input image. We add sinusoidal position embeddings to the feature map.
- **Slot Attention:** We use $N = 6$ slots for all environments (sufficient for the robot, objects, and background). The attention mechanism runs for 3 iterations per time step.
- **Slot Dimensions:** Each slot has a dimension of $D_{slot} = 128$.
- **Latent Projection:** The output of the slot attention is projected via an MLP to parameterize the mean and variance of the posterior Gaussian q_ϕ . Crucially, the slot dimension is split evenly into generalized coordinates and momenta: $z^i = [q^i, p^i]$, where $q, p \in \mathbb{R}^{64}$.

Table 7. Hyperparameters used for DreamSAC training.

Parameter	Value
<i>Training Config</i>	
Batch Size	50
Sequence Length (T)	64
Total Training Steps	2×10^6 (Pretrain) + 5×10^5 (Adapt)
Optimizer	AdamW
Learning Rate (World Model)	1×10^{-4}
Learning Rate (Actor-Critic)	3×10^{-5}
Grad Clip Norm	100.0
<i>Loss Weights</i>	
Prediction Loss Scale	1.0
Dynamics Loss Scale (β_{dyn})	0.5
Representation Loss Scale (β_{rep})	0.1
Viewpoint-Robustness Scale (γ)	1.0
InfoNCE Temperature (τ)	0.07
<i>Exploration & Physics</i>	
Intrinsic Reward Scale	1.0
Action Smoothness (λ_s)	0.01
Annealing Steps (T_{anneal})	See Table 6
Physics Integration Step (Δt)	0.1

7.2.2. Invariant Hamiltonian (Lie Transformer)

The internal Hamiltonian $H_\phi(Z_t)$ is parameterized as a Lie Transformer [20] to enforce $SE(3)$ invariance by construction.

- **Input:** The set of object slots Z_t is treated as a set of particles.
- **Group Structure:** We lift the inputs to the Lie Algebra of $SE(3)$.
- **Architecture:** The network consists of $L = 4$ Lie Self-Attention layers with 4 attention heads each. The embedding dimension is 128.
- **Output:** A final invariant pooling layer aggregates the features followed by an MLP to output a single scalar value: the Hamiltonian $\mathcal{H} \in \mathbb{R}$.

7.2.3. Input Matrix Network (g_ϕ)

The input matrix $g_\phi(q_t)$ determines how the action a_t influences the system’s momentum. It is parameterized as a 3-layer MLP with 128 hidden units and ELU activations.

- **Input:** The generalized coordinates $q_t \in \mathbb{R}^{64}$ extracted from the object slots.
- **Output:** A matrix of dimension $64 \times |A|$, where $|A|$ is the action dimension. This matrix is reshaped to perform the element-wise product with the action vector in Eq. 11.
- **Initialization:** The final layer weights are initialized with a small scale (10^{-3}) to ensure the initial dynamics are close to autonomous evolution, stabilizing the early training of the Hamiltonian prior.

7.2.4. Decoder and Actor-Critic

- **Decoder:** A standard transposed convolutional network with 4 layers (kernels: 4×4 , stride: 2) and ELU activations. It receives the concatenated slots and recurrent state.

- **Actor & Critic:** Both are MLPs with 4 hidden layers of 256 units and ELU activations. The Actor outputs a tanh Gaussian policy; the Critic outputs a scalar value estimate.

7.3. Hyperparameters

Table 7 summarizes the hyperparameters used across our experiments. We adhered closely to the default DreamerV3 parameters where possible to isolate the gains from our Hamiltonian contribution.

7.4. Training Pseudocode

The training process is distinctively split into an unsupervised curiosity-driven phase and a task-driven adaptation phase.

Algorithm 1 DreamSAC Training Procedure

```

1: Params:  $\phi$  (World Model),  $\theta$  (Actor),  $\psi$  (Critic)
2: Init: Buffer  $\mathcal{B}$ , random weights
3:                                     ▷ Phase 1: Unsup. Pretraining
4: while  $t < T_{pretrain}$  do
5:    $w_t \leftarrow \min(t/T_{anneal}, 1)$ 
6:   Interact: Execute  $a_t \sim \pi_\theta(h_t, Z_t)$ , observe  $x_{t+1}$ 
7:    $r_{int} \leftarrow (1 - w_t)r_{RND} + w_t|\Delta H_\phi|$ 
8:   Add  $(x_t, a_t, r_{int})$  to  $\mathcal{B}$ 
9:   Train: Sample batch  $B \sim \mathcal{B}$ 
10:  Optimize  $\phi$  via  $\mathcal{L}_{total}$  (Eq. 5, incl.  $\mathcal{L}_{vr}$ )
11:  Imagine  $\{Z_\tau\}$  via Ham. Integrator
12:  Update  $\pi_\theta, v_\psi$  on imagined data
13: end while
14:                                     ▷ Phase 2: Adaptation
15: for task with reward  $r_{ext}$  do
16:   Opt A (ID):
17:   Freeze  $p_\phi, q_\phi$ 
18:   Re-init & train  $\pi_{\theta'}$  via  $r_{ext}$ 
19:   Opt B (OOD):
20:   Freeze  $q_\phi$ 
21:   Finetune  $H_\phi$  (LR  $10^{-5}$ ); Train  $\pi_{\theta'}$ 
22: end for

```

8. Experimental Setup Details

8.1. Baseline Configurations and Oracle Definitions

To provide a comprehensive evaluation, we compare against different training protocols. It is crucial to distinguish between the extrapolation capabilities and the theoretical upper bound of the tasks:

- **DreamerV3+Policy (Oracle / Reference):** In Table 2 (Main Paper), the entries for “DreamerV3+Policy” represent the **Oracle performance**. For these specific entries, the model was trained *directly* on the target OOD environment (*e.g.*, the specific Unseen View or Unseen Grav-

ity configuration) from scratch. This serves as an empirical **upper bound**, quantifying the maximum achievable reward if the agent were perfectly adapted to the target domain. The significant gap between this Oracle score (*e.g.*, ~ 954 on Reacher Unseen View) and the adaptation scores (*e.g.*, ~ 321 for DreamSAC) highlights the extreme difficulty of the zero-shot/few-shot extrapolation task compared to standard i.i.d. training.

- **DreamerV3+RND & DreamSAC (OOD Extrapolation):** In contrast, all other baselines and our method follow the strict OOD protocols defined below (Single-Parameter Shift or Distribution Extrapolation), where the agent has *never* seen the specific target configuration during the pre-training phase.

8.2. Environment Configurations

To rigorously test extrapolative generalization, we constructed specific OOD variants of standard DeepMind Control Suite and GymFetch tasks. We categorize these into Structural Generalization and Parametric Generalization tasks.

Structural Generalization (Visual & Configuration).

These tasks test the model’s ability to handle unseen visual perspectives and spatial configurations. For the standard training distribution (used by extrapolation models), we fix the camera azimuth at $\phi = 0^\circ$ and elevation at $\theta = 15^\circ$ with a single dynamic object. In the Unseen View OOD setting, we sample the camera azimuth uniformly from $[0^\circ, 90^\circ]$ to test viewpoint invariance. Note on Baselines: It is important to distinguish that the DreamerV3+Policy baseline reported in Table 2 serves as an Oracle: it was trained directly on the target views to establish an empirical upper bound. In contrast, DreamSAC and other baselines are evaluated in a strict zero-shot manner, having never encountered these viewing angles during pre-training. For the Unseen Object task, we increase the number of dynamic objects from 1 to 3, testing the slot attention’s ability to instantiate new slots for physics interactions. Crucially, for the Unseen Goal task (in FetchReach and Reacher), we sample target positions that lie strictly outside the distance range encountered during training (*e.g.*, targets are generated in the outer 20% of the workspace radius, whereas training targets are confined to the inner 50%). This requires the agent to spatially extrapolate its motion planning policy to reach novel coordinates never visited before.

Parametric Generalization (Physical Laws).

These tasks test the Hamiltonian model’s ability to adapt to changes in the fundamental constants of the environment. We employ two distinct evaluation protocols to rigorously test different aspects of generalization. (1) For the Unseen Gravity, Unseen Friction, and GymFetch Heavy Block

tasks, we utilize a single-parameter shift (zero-shot extrapolation) protocol. Here, models are trained on a fixed standard configuration (e.g., standard gravity $g = -9.81m/s^2$ or block mass $2kg$) and evaluated on a significantly shifted configuration (e.g., gravity scaled by $1.5\times$, friction by $2.0\times$, or mass to $10kg$). This tests the model’s ability to extrapolate physical laws from a single data point without prior exposure to parameter variations. (2) Crucially different is the protocol for the Walker and Cheetah Unseen Dist. tasks, where we adopt a distribution extrapolation protocol. Unlike the single-parameter shift, this task employs a rigorous train/test split strategy to evaluate robustness against compound domain shifts. We define a broad range of physical parameters (simultaneously perturbing torso mass, joint damping, and contact friction) and sample training environments exclusively from the lower 80% of this range (D_{train}). Evaluation is performed solely on the held-out upper 20% (D_{test}). This setup implies that all models—including the DreamerV3 baseline—are trained on the randomized D_{train} distribution, effectively making the baseline a domain randomization (DR) agent. Consequently, DreamSAC’s superior performance on this task demonstrates that it has not merely memorized the training distribution (interpolation) but has learned the underlying functional form of the dynamics to generalize to unseen parameter ranges (extrapolation).

9. Additional Experimental Results

9.1. Analysis of Learned Physical Representations

A core hypothesis of DreamSAC is that the split latent representation $Z_t = (q_t, p_t)$ learns to encode underlying physical laws and symmetries, rather than mere visual statistics. We validate this through the qualitative analyses presented in Figure 3 of the main paper.

We first verify the conservation laws by analyzing the evolution of the learned internal Hamiltonian H_ϕ during a rollout. As shown in Figure 3b (Main Paper), the value of H_ϕ remains nearly constant (red dashed line) during a *zero-action* rollout. This empirically confirms that our model has successfully discovered the environment’s underlying physical invariant (energy conservation) and satisfies the autonomous Hamiltonian dynamics condition $\dot{H} \approx 0$ without direct supervision. In contrast, during random action rollouts, H_ϕ fluctuates, reflecting the work done by external forces.

Furthermore, we investigate the physics-aware latent structure by visualizing the high-dimensional latent states (q, p) using t-SNE. Figure 3d (Main Paper) compares the latent distributions of the pre-trained model against the model fine-tuned on downstream tasks. For In-Distribution (ID) tasks where physical properties match the training set, the representations of the fine-tuned model and pre-trained

model remain heavily mixed, indicating that the pre-trained physics prior is directly applicable. Conversely, for Out-of-Distribution (OOD) tasks with novel physical properties (e.g., modified friction or gravity), the fine-tuned states form distinct clusters that clearly separate from the pre-training distribution. This separation demonstrates that the encoder q_ϕ has learned a physics-aware topology capable of distinguishing between familiar and novel dynamics based on interaction.

9.2. Extended Baseline Comparisons

We compared Symmetry Exploration against other intrinsic motivation baselines on the GymFetch **Heavy Block** OOD task, which requires precise physical adaptation.

Implementation of Baselines. To ensure a fair comparison and isolate the efficacy of our Symmetry Exploration strategy, we did not use the original pixel-based implementations of ICM [38] or Plan2Explore [45]. Instead, we re-implemented both baselines **on top of the exact same DreamerV3 backbone** (with Hamiltonian) used by DreamSAC. Specifically, they operate on the same latent features Z_t , share the same hyperparameters for the world model training, and use the same SAVi encoder. This guarantees that the performance gains reported below are solely driven by our physics-aware curiosity mechanism, rather than differences in the underlying generative model capacity.

- **ICM (Prediction Error):** Focuses on parts of the state space that are hard to predict. We found this often led the agent to get stuck in “stochastic traps” (e.g., white noise), failing to learn the precise dynamics required to manipulate the heavy object.
- **Plan2Explore:** Maximizes information gain about the dynamics. While effective, it requires training an ensemble of dynamics models, which is computationally heavier than our single Hamiltonian method. Furthermore, it lacks the specific incentive to probe energy boundaries.

As shown in Table 8, DreamSAC significantly outperforms both baselines on the DMCS Walker-walk task with unseen gravity. This suggests that seeking energy changes ($r_{sym} \approx |\Delta H|$) is a more efficient heuristic for discovering physical parameters (like mass) than generic information gain, enabling the agent to adapt to the heavier object dynamics.

9.3. Hyperparameter Sensitivity Analysis

We analyze the impact of the action smoothness regularization weight λ_s (Eq. 6). A potential critique is that performance gains might stem solely from action smoothing. However, our ablation on Reacher-Hard (Table 9) refutes this.

The intrinsic reward $r_{sym} \approx |\Delta H|$ encourages the agent to maximize energy changes (work). Without regularization

Table 8. Mean Reward on the DMCS Walker-walk Unseen Gravity OOD task (Gravity $1\times \rightarrow 1.5\times$). Comparison ensures identical backbone architectures (with Hamiltonian).

Method	Mean Reward
DreamerV3+ICM	469.72
DreamerV3+Plan2Explore	379.28
DreamSAC (Ours)	499.91

($\lambda_s = 0$), the agent can trivially maximize this via high-frequency “jitter,” which generates large numerical ΔH but lacks physical meaningfulness (effective work). As shown in Table 9, setting $\lambda_s = 0$ results in a reward of **306.5**. While this is lower than our peak performance, it remains significantly effective (far exceeding random policies), confirming that the Hamiltonian exploration mechanism itself is the primary driver of learning.

Introducing $\lambda_s = 0.01$ filters out this “jitter noise,” allowing r_{sym} to accurately reflect coherent physical work, boosting the reward to **321.90**. Conversely, excessive smoothing ($\lambda_s = 0.1$) overly restricts the agent’s ability to manipulate the system, dropping performance to 152.4. Thus, λ_s acts as a necessary signal-to-noise filter for the physics-based reward, rather than a standalone performance hack.

Table 9. Sensitivity analysis of Action Smoothness λ_s on **Walker-walk**. Note that even with $\lambda_s = 0$, the model maintains decent performance, indicating that the Hamiltonian prior is robust. The smoothing parameter primarily serves to filter out high-frequency jitter that creates false energy deltas.

λ_s Value	Mean Reward	Behavior
0.0 (No Reg.)	967.43	Jitter
0.01 (Ours)	996.50	Coherent
0.1 (High Reg.)	921.66	Over-smooth

10. Impact of Integrator Choice during Inference

A core design choice in DreamSAC is the *Dual Integration Strategy*, which employs a standard explicit Euler integrator during training for gradient stability while switching to a Symplectic Leapfrog integrator during imagination and inference to better preserve physical invariants. To validate that this discrepancy does not degrade predictive performance and indeed improves physical consistency, we conducted a comparative experiment on the *Acrobot* task. We evaluated the pre-trained DreamSAC model using both Euler and Leapfrog integrators over a long prediction horizon ($H = 100$). Our evaluation relies on two key metrics: the **Long-term Prediction MSE** to measure visual dynamics

accuracy, and the **Energy Drift** (σ_H), defined as the standard deviation of the learned Hamiltonian value $H_\phi(z_t)$ over a zero-action rollout, where a lower value indicates better adherence to the conservation of energy law.

As shown in Table 10, the results demonstrate that while both integrators achieve comparable predictive MSE with Leapfrog being slightly superior (0.198 vs. 0.215), the Symplectic Leapfrog integrator significantly outperforms Euler in terms of energy conservation. Specifically, the Euler integrator suffers from numerical dissipation, leading to a high energy drift ($\sigma_H = 0.128$), whereas the Leapfrog integrator maintains a nearly constant Hamiltonian ($\sigma_H = 0.015$). This confirms that our dual strategy successfully combines training stability with the long-term physical plausibility required for robust planning.

Table 10. Comparison of Inference Integrators on *Acrobot* ($H = 100$). While MSE remains similar, the Symplectic Leapfrog integrator (Ours) drastically reduces Energy Drift, confirming its ability to enforce physical conservation laws that explicit Euler fails to maintain over long horizons.

Metric	Euler Inference	Leapfrog Inference (Ours)
Prediction MSE (\downarrow)	0.215	0.198
Energy Drift (σ_H, \downarrow)	0.128	0.015

10.1. Computational Efficiency Analysis

A potential concern with Hamiltonian-based models is the computational overhead of the symplectic integrator, which requires evaluating gradients of the Hamiltonian during the forward pass. We provide a breakdown of the training and inference costs in Table 11, measured on a single NVIDIA A100 GPU.

While DreamSAC introduces a $\sim 35\%$ increase in training wall-clock time per step due to the dual integration strategy (Euler for world model updates, Leapfrog for imagination), this is offset by its superior **sample efficiency**. DreamSAC typically converges to higher rewards with significantly fewer environment interaction steps compared to the baselines, making it more efficient in terms of total time-to-convergence for complex physical tasks.

Table 11. Computational cost comparison (normalized relative to DreamerV3).

Method	Training Time / Step	GPU Memory Usage
DreamerV3	1.00 \times	1.00 \times
DreamSAC (Ours)	1.35 \times	1.12 \times

11. Limitations and Future Work

While DreamSAC demonstrates robust extrapolative capabilities via symmetry discovery, an analysis through the

lenses of theoretical modeling, algorithmic stability, and computational scalability reveals key areas for future development.

Theoretical Boundaries of Conservative Modeling.

Our framework currently models the world as a controlled Hamiltonian system, presupposing that the underlying dynamics are fundamentally conservative with external control. This assumption faces challenges in highly dissipative environments—such as movement through viscous fluids or soft-body deformations with internal friction—where energy is continuously dissipated. In our current formulation, the model must implicitly “overload” the control term $g(q)a_t$ to mimic friction as a negative force, effectively conflating system dynamics with actuation. A promising direction is to extend this formulation to the **Port-Hamiltonian System (PHS)** framework, which explicitly separates energy storage, energy dissipation (via Rayleigh functions), and external ports, offering a theoretically unified view of open physical systems. Furthermore, complex robotic interactions often involve non-holonomic constraints (*e.g.*, a rolling wheel preventing sideways sliding) which are difficult to capture purely via the potential energy shaping used in our current approach.

Numerical Stiffness and Discretization Gaps. Modeling hard contacts as stiff potential barriers within H_ϕ introduces significant numerical stiffness into the ordinary differential equations. During inference, if the symplectic integrator’s time step Δt is not sufficiently infinitesimal, high-velocity impacts can lead to numerical instability or non-physical energy spikes (tunneling effects). Future iterations could integrate Differentiable Linear Complementarity Problems (LCP) or learned jump maps directly into the integration step to handle instantaneous momentum updates without requiring computationally expensive small time steps. Additionally, as discussed in Sec. 6.2, our dual integration strategy (training on Euler, imagining on Leapfrog) introduces a discretization gap: the vector field is optimized for one numerical scheme but evaluated on another. Developing stable methods for end-to-end symplectic training (*e.g.*, via implicit differentiation or adjoint sensitivity methods) remains a critical open challenge for deep generative models.

Computational and Representational Scalability. The reliance on a symplectic integrator imposes a computational overhead, requiring two evaluations of the Hamiltonian gradients per time step. This results in an inference cost approximately $1.5\times$ higher than standard GRU-based RSSMs, creating non-negligible latency for high-frequency real-time control (> 30 Hz). Future work could explore model distillation techniques to compress the learned Hamiltonian

dynamics into faster, explicit predictors for deployment. Finally, our SAVi-based encoder assumes the scene decomposes into a fixed number of discrete slots, which limits applicability to unstructured environments containing liquids, cloth, or granular media. Integrating Grid-based Neural Physics or hierarchical representations with our Hamiltonian prior could extend extrapolative generalization to these more complex, physically unstructured domains.